## *Web Summary Report*
## January 2016 – December 2016
## Phase VI

In the sixth stage of the project the studies were focused on the growth and characterization of multifunctional zinc oxide thin films. Nd-doped ZnO films with highly tunable properties were grown by pulsed electron beam deposition at different temperature on Si and c-cut single crystal substrates. In particularly, Nd-doped ZnO films have been obtained either as transparent semiconductor and photon energy converter or as highly conductor without energy conversion. Details about results obtained in this Phase can be found in following paper presented in the Dissemination section. In conclusion, the objectives of Phase VI were realized, resulting multifunctional zinc oxide thin films for applications.

**Dissemination**

M. Nistor, L. Mihut, E. Millon, C. Cachoncinlle, C. Hebert, J. J.Perrière, RSC Adv. **6**, 41465-41472 (2016) and in 7 communications at international conferences.

**Cite this: RSC Adv., 2016, 6, 41465**

# Tailored electric and optical properties of Nd doped ZnO: from transparent conducting oxide to photon down-shifting thin films

**M. Nistor[1,*], L.Mihut[2], E. Millon[3], C. Cachoncinlle[3], C. Hebert[4], J. Perrière[4]**

*[1]National Institute for Lasers, Plasma and Radiation Physics (NILPRP), L22 P.O. Box. MG-36, 077125 Bucharest-Magurele, Romania*
*[2]National Institute of Materials Physics (NIMP), Atomistilor Str. 105 bis, P.O. Box MG-7, 077125 Magurele-Ilfov, Romania*
*[3]GREMI, UMR 7344 CNRS-Université d'Orléans, 45067 Orléans Cedex 2, France*
*[4]Sorbonne Universités, UPMC Univ Paris 06, UMR 7588, INSP, F-75005, Paris, France*
*[5]CNRS, UMR 7588, INSP, F-75005, Paris, France*
*Coresponding author: mnistor@infim.ro

**Abstract**

Nd-doped ZnO films with highly tunable properties were grown by pulsed electron beam deposition at 500 °C on Si and c-cut single crystal substrates under oxygen gas. The effects of a slight change in the oxygen pressure ($10^{-2}$ – $2x10^{-2}$ mbar) on the composition, structure and physical properties of the films were studied. Films grown at $10^{-2}$ mbar present a low resistivity ($5x10^{-3}$ Ωcm) and high transparency in visible range and do not show any near-infrared emission due to $Nd^{3+}$ ions. On the contrary, films grown at $2x10^{-2}$ mbar have high resistivity (> 16 Ωcm), high optical transparency and near infrared emission of the $Nd^{3+}$ ions is observed under indirect excitation at 335 nm (i.e. absorption by the ZnO matrix and transfer to $Nd^{3+}$ ions). These significant changes in physical properties, leading from transparent conducting oxide to photon down-shifting thin films, are related to growth mode in pulsed-electron beam deposition.

**Keywords:** Nd-doped ZnO; thin films, ablation, pulsed-electron beam deposition; resistivity, photoluminescence, down-shifting

## 1. INTRODUCTION

In addition to its remarkable chemical and physical properties, ZnO present some other characteristics (biocompatibility, environmental stability, low cost due to large abundance) that make it versatile for numerous applications in various domains like transparent electronics, photovoltaic, spintronics [1, 2]. As a result, the growth of ZnO thin films has been widely studied by chemical and physical methods [3-7]. Recently, we have demonstrated that epitaxial ZnO films on various single crystal substrates can be obtained by an original method: pulsed-electron beam deposition (PED) [8], which has similar features with pulsed-laser deposition (PLD) method, and is particularly well adapted to the growth of oxide films of complex compositions [9]. On one hand, such PED ZnO films present original properties, for example a metal-insulator transition (MIT) at low temperature is mainly related to some specificities of the growth by PED [10], since such a MIT has never been reported to our knowledge in undoped ZnO film grown by PLD, sputtering or other deposition methods.

On the other hand, doping by well-chosen elements is largely used to alter or enhance physical properties or to induce a new one in oxide material [11-14]. Such an approach has been used with ZnO films in order to tune its conductivity by Al, Si or other dopant elements [15-17], to induce ferromagnetism by Co, Cr or Fe doping [12,18, 19], or to obtain ZnO based solar spectrum converter by rare earth doping [20-23]. Among these rare earth dopants, a particular interest has been evidenced with neodymium (Nd) which induces near-infrared emission about 900 nm which is compatible with silicon solar cells, while ZnO is frequently used as transparent layer [17, 20, 24]. Studies on Nd-doped ZnO thin films have been mainly focused on the challenging Nd incorporation into ZnO (due to the large difference in ionic radius of $Nd^{3+}$ and $Zn^{2+}$, 0.098 and 0.074 nm, respectively) and on the $Nd^{3+}$ photoluminescence characteristics, but their fundamental physical properties which may depend upon growth conditions remain insufficiently evaluated.

In this work we have studied the growth of Nd doped ZnO thin films by PED together with their properties. The aim of this paper is to demonstrate a simple way to tune the physical properties of Nd doped ZnO thin films by a precise control of the growth conditions (oxygen pressure). The composition and structure of these films were correlated to their optical and electrical properties. The results show that a slight difference in oxygen pressure, which does not lead to measurable changes in the film composition and crystalline state, has drastic effects on the film properties. Actually, due to a precise control of the growth parameters, abrupt changes are observed in the electrical conductivity and optical absorption of the films and in $Nd^{3+}$ ion related photoluminescence.

## 2. EXPERIMENTAL DETAILS

Nd-doped ZnO thin films were grown by PED on Si and c-cut sapphire single crystal substrates at 500°C substrate temperature under $O_2$ reactive gas at 2 x $10^{-2}$ mbar and 1 x$10^{-2}$ mbar pressure, respectively. The homemade PED set-up was described in previous papers [8-10]. Briefly, a 16 nF capacitor charged at 16 kV was discharged between a hollow cathode and a grounded anode (the vacuum chamber) through a capillary tube of 6 mm diameter and 105 mm length. A polyenergetic pulsed electron beam was produced of about 100 ns FWHM, with a fluence of about 2.5 J/cm$^2$ at the target surface and a 1 Hz repetition rate. The beam interacted at 45° angle of incidence with 1% at. Nd doped ZnO rotating target and the target-substrate distance was 40 mm.

The thickness and composition of films were determined by Rutherford backscattering spectrometry (RBS) under the Convention for SAFIR@ALTAIS between Université Pierre et Marie Curie and University of

Namur. Such measurements gave composition for the Nd and Zn cations with a rather good accuracy (better than 0.5%), while the oxygen content was only determined with a 4% accuracy, owing to the low RBS yield on light elements like oxygen. X-ray diffraction (XRD) analyses of the films were carried out in the symmetric Bragg-Brentano geometry using a four circles diffractometer (Philips Xpert MRD) with the Cu K$\alpha$ radiation ($\lambda$= 0.154 nm) from the PIMM – Arts et Metiers ParisTech in Paris. The electrical resistivity of thin films was performed by the four probe method, from room temperature to liquid helium and a MMR Technologies Inc. setup was used for Hall measurements system in the van der Pauw geometry at room temperature and 0.35 T [10]. The optical transmittance of the films was measured with a Varian Cary 5000 spectrometer. Photoluminescence emission (PL) and excitation (PLE) measurements were carried out using a Fluorolog 3-22 Horiba Jobin Yvon spectrometer at NIMP. The films were excited at room temperature using a 450 W Xenon lamp and a monochromator having 1200 grooves/mm. The near infrared photoluminescence signal (NIR PL) was analyzed by a monochromator with 600 grooves/mm and detected with a liquid nitrogen cooled InGaAs detector.

### 3. RESULTS and DISCUSSION

Previously, the properties of the oxide thin films grown by PED were found to be strongly dependent on the gas composition and pressure, electron beam parameters and substrate temperature [8-10]. In particularly, the current and energy of the pulsed-electron beam are depending on working gas pressure and external parameters, leading to an influence on the thin film quality [9]. Thus, in this work, two regimes in oxygen pressure were explored for the film growth, at $2x10^{-2}$ mbar (denoted high pressure regime, HP) and at $1 x 10^{-2}$ mbar (low pressure, LP), respectively.

Typical RBS spectra for films grown on Si substrate under HP and LP, respectively are presented in Fig. 1, while the quantitative results for all films are summarized in Table I. Fig. 1 shows that Nd is uniformly incorporated in the films depth without any interdiffusion with the Si substrate. Values of Nd concentrations are in the 1.1 to 1.2 % range (with respect to the Zn content), indicating a near stoichiometric transfer from target to film, whatever the substrate and oxygen pressure. An oxygen composition corresponding to the ideal stoichiometry ($Zn_{0.99}Nd_{0.01}O_1$) was deduced from the simulation of the RBS spectra whatever the oxygen pressure during the growth. However it has to be noticed that the accuracy of the oxygen determination by RBS is limited (about 4%), and thus a slight oxygen deficiency in the films (depending upon the oxygen pressure) cannot be excluded. The sole clear difference appearing between the films grown under LP and HP, respectively is the value of their thickness. Indeed the growth rate varies from 0.52 Å/s at HP pressure to 1.08Å/s at LP pressure, leading to film thickness of 270 nm and 420 nm, respectively. This should be related to some differences in the PED growth mode as function of the oxygen pressure.

The inset in Fig. 1a represents a typical XRD θ-2θ pattern recorded on a Nd doped ZnO film**.** This diagram only shows the (002) reflection peak of the ZnO wurtzite structure meaning that the film is highly c-axis oriented as it can be expected [8, 10]. Similar results were obtained for all the films, and the values of the c-axis parameter deduced from such XRD patterns are presented in Table I. These values only show slight variations with respect to that of the undoped ZnO film grown by PED on c-cut sapphire at 500 °C (0.5258 nm) [8] and bulk value (0.52066 nm). Moreover the crystallite size estimated through the Scherrer formulae from the (002) FWHM peak is lower than the typical value measured on undoped ZnO film grown under similar conditions (22 nm). The reason why could be the fact that at 500°C, Nd segregation towards grain boundaries can occur in ZnO, as it has been previously reported [24, 25]. This segregation would limit the size of the crystallites in the Nd doped ZnO films [24]. This also means that only a fraction of the Nd ions are incorporated in the ZnO network, and this could explain the fact that the c-axis parameter does not show a large variation.

Asymmetric XRD analyses, i.e. pole figure measurements (not presented here) revealed an epitaxial growth of Nd-doped ZnO films on c-cut sapphire substrates with classical "30° rotation" epitaxial relationship of ZnO on sapphire as it has already been reported [8, 26], while films grown on Si show only c-axis texture. It can thus be concluded that large differences in the film composition and structure are not evidenced as a function of the growth conditions.

The electrical properties of the films were checked and Hall measurements were carried out at room temperature for the films grown on c-cut sapphire substrate. These measurements indicated, that as expected, Nd-doped ZnO films are n-type. Their resistivity of the films, carrier concentration and mobility are presented in Table II.

This Table shows that a very large difference exists in the values of the film resistivity ρ. Indeed for the film grown at HP, ρ was found more than $10^3$ times higher than that of the film grown at LP. This large difference is essentially due to a decrease in carrier density and mobility (Table II). Moreover, these mobility values are relatively low, strongly dependent upon the scattering centres (defects, ionized impurities, grain boundaries…) present in the films [4]. It has been deduced from the XRD analysis that the crystalline state and crystallite size are very similar for the HP and LP films, and this cannot explain the low values of the carrier mobility in the two types of films.

The large difference in carrier concentration in the LP and HP films cannot be attributed *a priori* to a single phenomenon. Nd should act as an impurity in ZnO, i.e. as a donor dopant, occupying divalent Zn sites and giving an electron to the ZnO lattice. Actually, both the presence of $Nd^{3+}$ in substitution of $Zn^{2+}$ in the ZnO matrix and of native defects such as oxygen vacancy and zinc interstitial must be taken into account. We cannot *a priori* exclude the fact that the fraction of Nd electronically active in the film decreases with increasing oxygen pressure. In addition the increase of carrier concentration can be related to an increase of oxygen vacancies in the film. Despite that no oxygen depletion is evidenced by RBS due to the accuracy of oxygen atoms by this technique, the oxygen vacancy concentration is certainly higher in the LP films than in the HP one. The slight change in oxygen pressure may induce some effects in the PED process. Actually, although in both low and high pressure regimes the electron energy distribution of the beam is poly-energetic, with a majority of electrons having low and medium energies in the few keV range, their ratio differs in function of the pressure [9]. This leads to an energy deposition profile into the target slightly different according to the pressure. Both the amount and energy of species emitted by the target during electron interaction would be different. A higher amount of species will reach the substrate in the LP regime with respect to the HP regime. As a result, the deposition rate will be higher in this regime and the incorporation of oxygen in the film will be lower, i.e. a higher concentration of oxygen vacancies could be expected in the LP film in comparison with the HP film [27]. In this frame, a slight (1%) oxygen vacancy concentration in the LP film (which could not be measured by RBS) would lead to a carrier density in the $10^{20}$ $cm^{-3}$ range, i.e. a value sufficient to explain the low resistivity of the LP film.

Temperature dependent resistivity curves ρ(T) were measured for the Nd-doped ZnO films and Fig. 2 summarizes these results. Tunable electrical resistivity was obtained, varying few orders of magnitude.

Nd-doped ZnO thin film grown at HP shows a semiconducting behaviour down to ~ 150 K where the resistivity becomes too high to be measured in the four probe setup. In contrast, the film grown at LP shows also an increasing resistivity down to liquid He but with the ρ(4K)/ρ(300K) ratio about 1.3, which does not correspond to the variation expected for a classical semiconductor presenting a thermally activated electronic transport. In such a case, it is interesting to look at the value of parameter $k_f\Lambda$, with $k_f$ being the Fermi momentum and Λ the electronic mean free path [28].

$$k_f \Lambda = \hbar (3\pi^2)^{2/3} / (e^2 \rho n^{1/3})$$

As previously noted [28, 29], for $k_f\Lambda >> 1$ the system presents a metallic behaviour, and for $k_f \Lambda << 1$ the system is insulating, i.e. strongly localized [30], a metal to insulator transition being expected if $k_f\Lambda$ is close to unity. Table II clearly shows that the HP film is in the strong localization regime due to the low value of carrier density and its high resistivity. On the contrary the LP film is on the metallic side of the metal – insulator transition owing to its high carrier density (1.35 $10^{20}$ $cm^{-3}$) largely exceeding the Mott critical density (from 1 to 5 x $10^{19}$ $cm^{-3}$ for undoped ZnO [29]) and to its low resistivity, being a heavily degenerate semiconductor with Fermi level lying in the conduction band.

For the HP film (Fig. 3a), the Arrhenius law versus temperature for thermal activated transport mechanism from room temperature to 246 K explains the semiconducting behaviour as it is classically observed for ZnO thin films. The activation energy of $E_a$=11.4 meV was estimated from the slope of the linear region of the plot ln ρ = f (1/T) and is shown in the inset of Fig. 3. This value is comparable to that measured for undoped and doped ZnO films [8, 31].

For the LP film, although the $k_f\Lambda$ value would indicate that the electronic state of the film is on the metallic side of the MIT, the temperature coefficient (TCR) remains slightly negative as observed in its ρ(T) curve (Fig. 2). This negative TCR has to be related to the structural disorder in the film [28-29]. Indeed, a negative TCR may occur in the metallic side of a semiconductor - metal transition due to the scattering of the carriers by the defects present in the films. The resulting increase in resistivity can be described in the frame of the quantum corrections to conductivity model which correspond to the weak localization and enhanced electron interactions [10, 32].

Optical transmittance measurements for Nd-doped ZnO films and c-cut sapphire were performed in the 200-3200 nm range (Fig. 4a) in order to check their properties for photovoltaic applications, which requires transparency in visible and NIR domains. All these films have a transmittance higher than 80% in the visible wavelength range, including the sapphire substrate contribution, while in the IR domain a large difference between the two types of films is observed, depending on the oxygen pressure (thus electron density). High IR transmission ~80% at 2500 nm is observed for the HP film due to its low carrier density, while IR transparency decreases to about 60% at 2500 nm and is attributed to absorption by free carriers, correlated with three order of magnitude of the carrier density increase (Table II). A blue shift of the fundamental absorption is also observed for high electron density.

The absorption coefficient ($\alpha$) was calculated using the relation $\alpha = (1/d)\ln[(1-R)/T]$, where T is the transmittance, R is the reflectance (neglected here) and d is the film thickness. Fig. 4b shows the Tauc plot, i.e. $(\alpha E)^2$ vs. E, where E is the photon energy and $\alpha$ is the optical absorption coefficient, from which the optical band gap was estimated by extrapolating the linear part of the absorption edge to the intersection with energy axis, supposing that Nd-doped ZnO films have a direct band gap ($E_{gap}$). As the oxygen partial pressure increases, the band gap decrease in the range from 3.30 eV for the conducting Nd doped ZnO films grown at LP to 3.27 eV for the films grown at HP. This change in the optical absorption edge ($E_{gap}$) can be understood as a function of the respective carrier concentrations in the HP and LP films.

In the present case, the value of $E_{gap}$ (3.27 eV) for the HP film is close to the bandgap (3.28 eV) measured in undoped ZnO films grown by PED at 500 °C [8]. Therefore, no noticeable Burstein-Moss effect is observed in this film as expected for the measured very low carrier density (about 4x$10^{17}$ $cm^{-3}$).

For the LP film, the $E_{gap}$ value is related to the fact that this film is on the metallic side of the MIT as shown above. In fact, for carrier density larger than the critical carrier density of ZnO ($n_c$ = 1 - 5 x$10^{19}$ $cm^{-3}$ [29]), the increase in optical band gap is well described by the Burstein-Moss effect (BM) [28, 33-36]. Then for increasing carrier density > $n_c$, when the donor band merges with the conduction band as a characteristic of the semiconductor – metal transition, the shift in $E_{gap}$ decreases due to the band gap renormalization effect (BGR). Then for further increasing carrier density, $E_{gap}$ will further increase at different rate. For the LP film, the carrier density (1.35 $10^{20}$ $cm^{-3}$) is higher than $n_c$ indicating that the LP film is on the increasing

branch following the band gap renormalization [35, 36]. Considering these competing effects, widening and narrowing (shrinkage) of the gap, the shift of $E_{gap}$ is given by [35-37]:

$$E_{gap} = E_{gap\ ZnO} + \Delta E_{BM} - \Delta E_{BGR} \quad (2)$$

where $E_{gap\ ZnO}$ is the gap of undoped ZnO (3.28 eV used in this work).

The BM effect which is due to a shift of Fermi level inside the conduction band was estimated from [37]:

$$\Delta E_{BM} = \left(\frac{h^2}{8\mu}\right)\left(\frac{3n}{\pi}\right)^{2/3}$$

where $\mu=(m_e^* m_h^*)/(m_e^* + m_h^*)$ is the reduces mass, $m_e^*=0.38m_0$ and $m_h^*=1.8\ m_0$ [37] are the effective mass of electron and hole for ZnO, $m_0$ is free electron mass (5.67 x $10^{-16}$ eV $cm^{-2}s^2$), h Planck constant and n electron density.

A value of $\Delta E_{BM}$=0.3 eV was estimated for the 1.35x$10^{20}$ $cm^{-3}$ carrier density in LP Nd doped ZnO films, then Eq. (2) was used to obtain the value of $\Delta E_{BGR}$ about 0.1 eV for the experimental value of $E_{gap}$=3.30 eV.

To investigate the role of $Nd^{3+}$ ions in ZnO thin films, NIR PL spectra were measured at room temperature under excitation at 335 nm (i.e. photon energy higher than ZnO band gap) with a 10 µm excitation slit and a 10 µm emission slit. Fig 5a shows such a NIR PL emission spectrum of Nd ZnO films grown at 500°C on c-cut sapphire substrates under HP, while NIR PL for films grown under LP was not observed.

Under that indirect excitation, the spectrum recorded for the HP film shows two excited NIR PL bands centred around 920 nm and 1082 nm, corresponding to radiative relaxations from $^4F_{3/2}$ to its multiplets, i.e. well-known $^4F_{3/2} \rightarrow {}^4I_{9/2}$ (~940 nm) and $^4F_{3/2} \rightarrow {}^4I_{11/2}$ (1064 nm) transitions of $Nd^{3+}$ ions [20, 38]. Similar results were obtained for the films grown on Si or c-cut substrates, evidencing that the PL properties are not depending on the epitaxy, thin films having a c-axis texture are enough for applications.

Theoretically five spectral resolved emission bands/peaks for the $^4F_{3/2} \rightarrow {}^4I_{9/2}$ transition would be expected in Fig. 5a for $Nd^{3+}$ luminescence centers in the ZnO crystal, i.e. for a well-ordered crystalline environment around $Nd^{3+}$ ions in ZnO lattice. However, at higher spectral resolution, the experimental spectrum of the $^4F_{3/2} \rightarrow {}^4I_{9/2}$ transition of the film grown at HP, recorded with a 10 µm excitation slit and a reduced 5 µm emission slit (Fig. 5b), shows three distinct bands already seen in Fig. 5a together with other small contributions which are not well spectrally resolved or indicating a partially-ordered crystalline environment around $Nd^{3+}$ ions in ZnO [20, 38, 41]. The position of peaks is indicated in Fig. 5b. Similar situation was observed for the $^4F_{3/2} \rightarrow {}^4I_{11/2}$ transition (not shown). Moreover, the separation of different optically active sites for $Nd^{3+}$ in ZnO was not possible even by measurements of PL NIR and PLE at low temperatures [20, 38].

The NIR PL shape is very similar with those measured at room temperature either for Nd doped ZnO thin films grown by RF sputtering [20] or Nd doped ZnO nanocrystals [38], proving that $Nd^{3+}$ is optically active in the ZnO film host. This infrared emission, which covers the spectral range useful for solar cell applications, was attributed to an energy transfer from ZnO matrix to the $Nd^{3+}$ ions that are incorporated into ZnO lattice [20, 38, 39].

In order to gain more information, the excitation spectrum of the PL emission (PLE) in the range of 285-950 nm was recorded at room temperature for both intense $Nd^{3+}$ ion transitions observed in HP Nd doped ZnO films. In Fig. 6 the PLE spectrum for the 1082 nm $Nd^{3+}$ peak is shown with continuous line, together with the spectral distribution of the Xe lamp intensity recorded by a photodiode (dash dot line). Both spectra are normalised in intensity for comparison purpose.

The PLE spectrum follows the absorption edge of ZnO below 400 nm, proving that the energy transfer occurs from the ZnO host to Nd ions. Despite the Xe lamp spectrum, which contributes to entire

spectral region, the presence of small $Nd^{3+}$ peaks in the spectrum shows that above 400 nm these peaks corresponds to their direct excitation, evidencing the strong crystal field experienced by $Nd^{3+}$ in the ZnO lattice [20, 38, 39]. Similar spectra were recorded in films and nanocrystals, slightly shifts in position of some peaks being noticed [20, 38, 39]. As reported, the wide absorption region of ZnO increases the advantage of indirect excitation in respect with direct excitation.

From the XRD and RBS analysis it was shown that the Nd composition, crystalline state and crystallite size are very similar for the HP and LP films, thus the drastic differences observed in NIR PL spectra (Fig. 5a) cannot be ascribed to them. On contrary, the drastic differences in optical and electrical properties of the films could contribute to a tentative explanation.

In ref. [40] it was proposed a universal behaviour model of the valence stability of lanthanide ions, which is related to the position of $4f^n$ ground state of lanthanide in respect to the Fermi energy of the inorganic host. In this model, the Fermi level was assumed to be located midway between the top of the filled valence band and the bottom of the empty conduction band. If a reducing atmosphere that adds electrons to ZnO, is assured during the growth, $Nd^{3+}$ may be converted to $Nd^{2+}$ ion. The Fermi level is rising towards conduction band, occupied levels in the divalent state being lower than it.

In the case of LP Nd-doped ZnO film, the Hall effect measurements showed that it is a heavily degenerate semiconductor with Fermi level lying in the conduction band. (Generally, for a n-type TCO, the location of the Fermi level between the top of the filled valence band and the bottom of the empty conduction band depends on the carrier density). From band gap shift estimation (transmittance measurements), the Fermi level is approximately located at about 0.2 eV inside the conduction band. According to the previous model, these conditions add electrons to ZnO, and $Nd^{3+}$ is converted to $Nd^{2+}$ for which occupied levels (in the divalent state) are located lower than the position of the Fermi level. Recently, the electronic structure of lanthanide impurities in ZnO was tentatively proposed [40] and according to that the divalent ground state of Nd is located inside the conduction band and the trivalent Nd inside the valence band. On the other hand it will be difficult to stabilize $Nd^{2+}$ in ZnO [39, 40]. These hypotheses lead to inappropriate conditions for the $Nd^{3+}$ ion formation in Nd-doped ZnO films grown at LP and thus it could explain the absence of the NIR PL under indirect excitation of the ZnO host.

On contrary, an oxidizing atmosphere may lower the Fermi energy and the divalent charge state could be converted to the trivalent one [39]. Under oxidizing atmosphere, i.e. growth of Nd doped ZnO films at HP, the Fermi level is lowering toward valence band and the divalent charge state is converted to the trivalent one. Thus PL NIR is observed only for the films grown at HP, suggesting the existence of a number of active $Nd^{3+}$ ions with energy transfer efficiency from the ZnO host.

It has to be noticed that tuning the physical properties of some oxide materials via a slight change in the oxygen pressure during the growth process have been reported in the case of other oxide materials [42-47]. Indeed abrupt changes in the optoelectronic properties of sputtered $MoO_x$ films have been observed by increasing the oxygen partial pressure from $1\ 10^{-3}$ mbar to $1.37\ 10^{-3}$ mbar during the sputtering process, the resistivity varying from $1.6\ 10^{-5}$ to 3.22 Ωcm [42]. In the same way a large variation in resistivity was observed for $In_2O_3$ thin films grown by PED [43] only by controlling the incorporation of oxygen in films during cooling process. Similar results on abrupt increase in resistivity together with a decrease in mobility were obtained for the growth of Ga-doped ZnO thin films [44] and undoped ZnO thin films [46] by pulsed-laser deposition as a function of oxygen pressure during growth and explained by variation of oxygen vacancy concentration [44]. Moreover, a significant shift of the Fermi level of +0.6 eV, measured by in situ X-ray photoelectron spectroscopy and ultraviolet photoelectron spectroscopy, was correlated with an abrupt resistivity increase for a slight oxygen variation from $10^{-1}$ to $3.3\ 10^{-2}$ mbar pressure during growth of undoped ZnO film by pulsed-laser deposition [45].

## 4. CONCLUSION

Influence of a slight variation in oxygen pressure on the stoichiometry, structure and optoelectronic properties of Nd doped ZnO films grown by PED have been studied. The slight change in oxygen pressure from 1 x $10^{-2}$ to 2 x $10^{-2}$ mbar has a strong impact on the physical properties of these films whereas measurable differences in the composition and structural characteristics of the films were not evidenced. Thus, the film resistivity varies from 5x$10^{-3}$ (for the LP film) to 16 Ωcm (for the HP film). Photoluminescence results show that highly resistive (semiconducting) transparent HP films could be efficient in the solar spectrum conversion (down-shifting) since photon in the UV domain are absorbed by the ZnO matrix and their energy is easily transferred to the $Nd^{3+}$ ions which further emit photon in the visible or NIR domains. On the contrary, the LP films which show a high transparency and conductivity do not play the role of energy converter. Actually, NIR PL of $Nd^{3+}$ in the LP films does not exist and this has to be related to a slight increase in the oxygen vacancies in this film. Oxygen vacancies in the Nd-doped ZnO films could change the crystalline field but this would only lead to a broadening of the $Nd^{3+}$ emission. The absence of $Nd^{3+}$ PL in this film therefore means that the energy transfer from the ZnO matrix to $Nd^{3+}$ ions does not occur in this case. The reason why the presence of oxygen vacancies block the energy transfer from the ZnO matrix to the $Nd^{3+}$ ions is not yet clearly understood. In this work a tentative explanation is based on the shifting of the Fermi level inside the conduction band for LP Nd-doped ZnO films, which favours the formation of the divalent state for $Nd^{2+}$ ions instead of $Nd^{3+}$ ions which are required for NIR PL properties.

In summary, this work shows that Nd-doped ZnO films can be tuned either as transparent semiconductor and photon energy converter or as highly conductor without energy conversion. It follows that multifunctional oxide films having both properties (transparent conductor and energy converter) could be obtained by co-doping ZnO films with Nd (for the energy conversion) and Al or Ga to increase the conductivity of such films. This work demonstrates thus that PED is a viable growth method for tuning the optical and electrical properties of oxide films which can be exploited in the field of optoelectronics or photovoltaic applications.

**Acknowledgements:** M. Nistor would thank a grant of the Romanian National Authority for Scientific Research, CNCS–UEFISCDI, project number PN-II-ID-PCE-2011-3-0566. W.Seiler is acknowledged for XRD measurements. The RBS measurements were performed under the Convention for SAFIR@ALTAÏS between the Université Pierre et Marie Curie and the University of Namur.

**References**

[1] H. Morkoç and Ü. Özgür, *Zinc Oxide: Fundamentals, Materials and Device Technology*, WILEY-VCH, 2009.
[2] K. Ellmer, *Nat. Photon*., 2012, **6,** 809.
[3] S.J. Pearton, W.H. Heo, M. Ivill, D.P. Norton, T. Steiner, *Semicon. Sci. Technol.*, **19**, 2004, R59
[4] P. Fons, K. Iwata, S. Niki, A. Yamada, K. Matsubara, *J. Cryst. Growth*, 1999, **201**, 627.
[5] S. Fay, L. Feitknecht, R. Schluchter, U. Kroll, E. Vallat-Sauvain, A. Shah, *Solar Energy Mat. Solar Cells*, 2006, **90**, 2960.
[6] J.H. Lee, K.H. Ko, B.O. Park, *J. Cryst. Growth*, 2003, **247**, 119.
[7] C. Florica, N. Preda, M. Enculescu, I. Enculescu, *Phys. Status Solidi RRL*, 2014, **8,** 648.
[8] S. Tricot, M. Nistor, E. Millon, C. Boulmer-Leborgne, N.B. Mandache, J. Perrière, W. Seiler, *Surface Science*, 2010, **604**, 2024.
[9] M. Nistor, N.B. Mandache, J. Perrière, *J. Phys. D-Applied Physics*, 2008, **41**, 165205.
[10] M. Nistor, N.B. Mandache, J. Perrière, C. Hebert, F. Gherendi, W. Seiler, *Thin Solid Films*, 2011, **519**, 3959.

[11] M. Orita, H. Hiramatsu, H. Ohta, M. Hirano, H. Hosono, *Thin Solid Films*, 2002, **411**, 134.
[12] H.J. Von Bardeleben, N. Jedrecy, J.L. Cantin, *Appl. Phys. Lett.*, 2008, **93**, 142505.
[13] P.A. Atanasov, R.I. Tomov, J. Perrière, R.W. Eason, N. Vainos, A. Klini, A. Zherikhin, E. Millon, *Appl. Phys. Lett.*, 2000, **76**, 2490.
[14] Y. Furubayashi, T. Hitosugi, Y. Yamamoto, K. Inaba, G. Kinoda, Y. Hirose, T. Shimada, T. Hasegawa, *Appl. Phys. Lett.,* **86**, 252101.
[15] O. Bamiduro, H. Mustafa, R. Mundle, R.B. Konda, A.K. Pradhan, *Appl. Phys. Lett.,* 2007, **90**, 242108
[16] C. Faure, J. Clatot, L. Teule-Gay, G. Campet, C. Labrugere, M. Nistor, A. Rougier, *Thin Solid Films*, 2012, **524**, 151.
[17] V. Bhosle, A. Tiwari, J. Narayan, *Appl. Phys. Lett.*, 2006, **88**, 032106.
[18] N. Jedrecy, H.J. Von Bardeleben, D. Demaille, *Phys. Rev. B*, 2009, **80**, 205204.
[19] M. Venkatesan, C.B. Fitzerald, J.G. Lunney, J.M.D. Coey, *Phys. Rev. Lett.*, 2004, **93**, 177206.
[20] M. Balestrieri, S. Colis, M. Gallart, G. Ferblantier, D. Muller, P. Gilliot, P. Bazylewski, G. S. Chang, A. Slaoui, A. Dinia, *J. Mat. Chem. C*, 2014, **2,** 9182.
[21] M. Subramanian, P. Thakur, S. Gautam, K.H. Chae, M. Tanemura, T. Hihara, S.Vijayalakshmi, T. Soga, S.S. Kim, K. Asokan, R. Jayavel, *J. Phys. D: Appl. Phys.*, 2009, **42,** 105410.
[22] G. Gottardi, R. Pandiyan, V. Micheli, G. Pepponi, S. Gennaro, R. Bartali, N. Laidani, *Mat. Sci. Eng. B*, 2013, **178,** 609.
[23] M. Balestrieri, G. Ferblantier, S. Colis, G. Schmerber, C. Ulhaq-Bouillet, D. Muller, A. Slaoui, A. Dinia, *Solar Energy Mat. Solar Cells*, 2013, **117**, 363.
[24] M. Nistor, E. Millon, C. Cachoncinlle, W. Seiler, N. Jedrecy, C. Hebert, J. Perrière, *J. Phys. D-Applied Physics*, 2015, **48**, 195103.
[25] J.C. Ronfart-Haret, J. Kossanyi, *Chem. Phys.*, 1999, **241,** 339.
[26] V. Craciun, R.K. Singh, J. Perrière, J. Spear, D. Craciun, *J. Electrochem. Soc.*, 2000, **147**, 1077.
[27] N. Chaoui, E. Millon, J.F. Muller, P. Ecker, W. Bieck, H.N. Migeon, 1999, *Mat. Chem. Phys.*, **59**, 114
[28] A.K. Das, R.S. Ajimsha, L.M. Kukreja, *J. Appl. Phys.*, 2014, **115**, 193705.
[29] M. Snure, A Tiwari, *J. Appl. Phys.,* 2009, **106**, 043904.
[30**]** N.F. Mott, *Conduction in Non-Crystalline Materials*, Clarendon, Oxford, 1993.
[31] S. Y. Myong, J. Steinhauser, R. Schlüchter, S. Faÿ, E. Vallat-Sauvain, A. Shah, C. Ballif, A. Rüfenacht, *Solar Energy Mat. Solar Cells*, 2007, **91**, 1269.
[32] R. Mundle, A.K. Pradhan, *J.Appl. Phys.*, 2014, **115**, 183503.
**[**33] Z. Qiao, C. Agashe, D. Mergel, *Thin Solid Films*, 2006, **496,** 520.
[34] J. Clatot, M. Nistor, A. Rougier, *Thin Solid Films*, 2013, **531**, 197.
[35] A.P. Roth, J.B. Webb, D.F. Williams, Solid State Comm. 1981, **39**, 1269.
[36] J. G. Lu, S. Fujita, T. Kawaharamura, H. Nishinaka, Y. Kamada, T. Ohshima, Z. Z. Ye, Y. J. Zeng, Y. Z. Zhang, L. P. Zhu, H. P. He and B. H. Zhao, *J. Appl. Phys.*, 2007, **101**, 083705.
[37] J. Kumar, A. M. Srivastava, *J. Appl. Phys.*, 2014, **115**, 134904.
[38] Y. Liu, W. Luo, R. Li, X. Chen, *J. Nanosci. Nanotechnol.*, 2010, **10,** 1871.
**[**39] Y. Liu, W. Luo, R. Li, H. Zhu, X. Chen, *Optics Express*, 2009, **17**, 9748.
[40] P.Dorenbos, *Chem.Mater.*, 2005, **17**, 6452.
[41**]** P.Dorenbos, *ECS J. Solid State Sci. Technol.*, 2014, **3,** R19
[42] A.L. Fernandes Cauduro, Z.E. Fabrim, M. Ahmadpour, P.F.P. Fichtner, S. Hassing, H.G. Rubahn, M. Madsen, *Appl. Phys. Lett.*, 2015, **106**, 202101.
[43] W. Seiler, M. Nistor, C. Hebert, J. Perrière, *Solar Energy Mat. Solar Cells*, 2013, **116**, 34.
[44] L. M. Wong, S. Y. Chiam, J. Q. Huang, S. J. Wang, J. S. Pan and W. K. Chim, *Appl. Phys. Lett.*, 2011, **98**, 022106.

[45] C.-H. Min, S. Cho, S.-H. Lee, D.-Y. Cho, W. G. Park, J. G. Chung, E. Lee, J. C. Lee, B. Anass, J. H. Lee, C. S. Hwang,S.-J. Oh, *Appl. Phys. Lett.*, 2010, **96**, 201907.
[46] S. Choopun, R. D. Vispute, W. Noch, A. Balsamo, R. P. Sharma, T. Venkatesan, A. Iliadis, D. C. Look, *Appl. Phys. Lett.*, 1999, **75**, 3947.
[47] S. S. Kim, B.T. Lee, *Thin Solid Films*, 2004, **446**, 307.

**TABLE CAPTION**

Table 1 : Growth conditions, composition and structural properties of Nd-doped ZnO thin films grown at 500°C under LP and HP

Table II : Electrical and optical properties of Nd-doped ZnO thin films grown at 500°C under LP and HP

| **growth conditions** | | **composition and growth rate** | **c-axis parameter (nm)** | | **crystallite size (nm)** | |
|---|---|---|---|---|---|---|
| **Substrate** | | **-** | **Si** | **c-cut** | **Si** | **c-cut** |
| 500°C | 1 $10^{-2}$ mbar LP | $Zn_{0.988}Nd_{0.012}O_1$ 0.52 Å/s | 0.5195 | 0.5194 | 12.0 | 12.2 |
| | 2 $10^{-2}$ mbar HP | $Zn_{0.989}Nd_{0.011}O_1$ 1.08Å/s | 0.5193 | 0.5207 | 12.3 | 12.7 |

**Table I**

| **growth conditions** | | **Resistivity ρ (Ωcm)** | **Mobility μ ($cm^2$/Vs)** | **Carrier density n ($cm^{-3}$)** | **$k_f\Lambda$** | **$E_g$ (eV)** |
|---|---|---|---|---|---|---|
| 500°C | 1 $10^{-2}$ mbar LP | 5.73 $10^{-3}$ | 8.10 | 1.35 $10^{20}$ | 1.34 | 3.30 |
| | 2 $10^{-2}$ mbar HP | 16.03 | 3.81 | 4.0 $10^{17}$ | 0.003 | 3.27 |

**Table II**

**FIGURE CAPTION**

Fig. 1
RBS spectra of the Nd-doped ZnO thin film grown on a Si substrate at 500 °C under HP (a) and LP (b), respectively. The inset of (a) shows the corresponding θ-2θ XRD pattern.
Fig. 2
Resistivity as function of temperature for Nd-doped ZnO thin films grown at LP (red symbols) and HP (black symbols). The resistivity scale is different for LP and HP films.
Fig. 3
Resistivity as function of temperature for Nd-doped ZnO thin films grown at HP. The inset shows the Arrhenius plot of resistivity, and the slope of the straight line lead an activation energy of $E_a$ = 11.4 meV
Fig. 4a
Transmittance of the Nd-doped ZnO films grown on c-cut sapphire substrate at HP and LP, respectively.
Fig. 4b
Variation of $(\alpha E)^2$ versus photon energy, E
Fig. 5a
NIR PL emission spectra under 355 nm excitation of Nd-doped ZnO thin films grown at LP and HP with 10 µm excitation slit and a 10 µm emission slit
Fig 5b
NIR PL emission spectra of Nd-doped ZnO thin film grown at HP under 355 nm excitation and with 10 µm excitation slit and a 5 µm emission slit
Fig 6
Room temperature PLE spectrum of the HP Nd-doped ZnO film. The dash dot line represents the spectral distribution of the Xe lamp intensity recorded by a photodiode

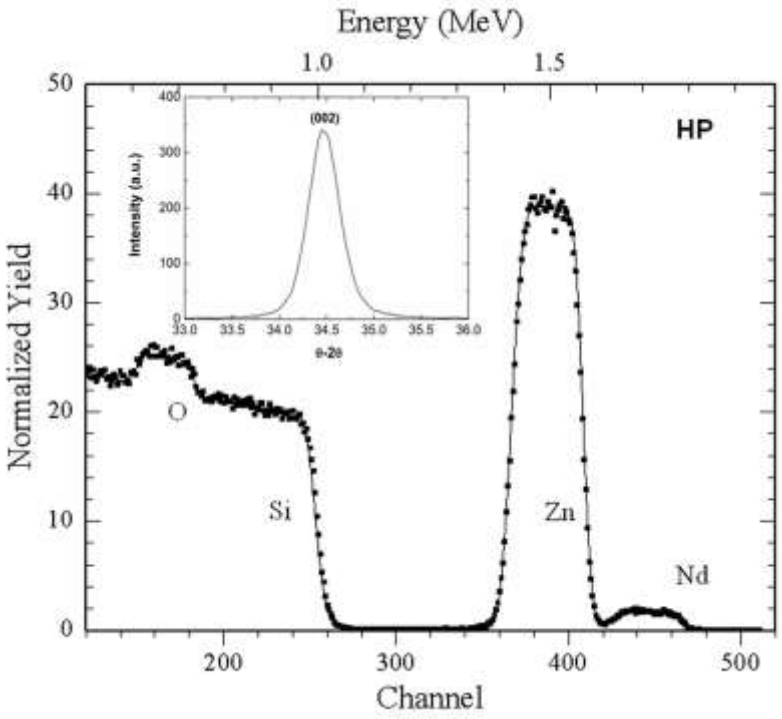
Energy (MeV)
1.0
1.5
HP
Normalized Yield
Channel
O
Si
Zn
Nd
(002)
Intensity (a.u.)
θ-2θ

a

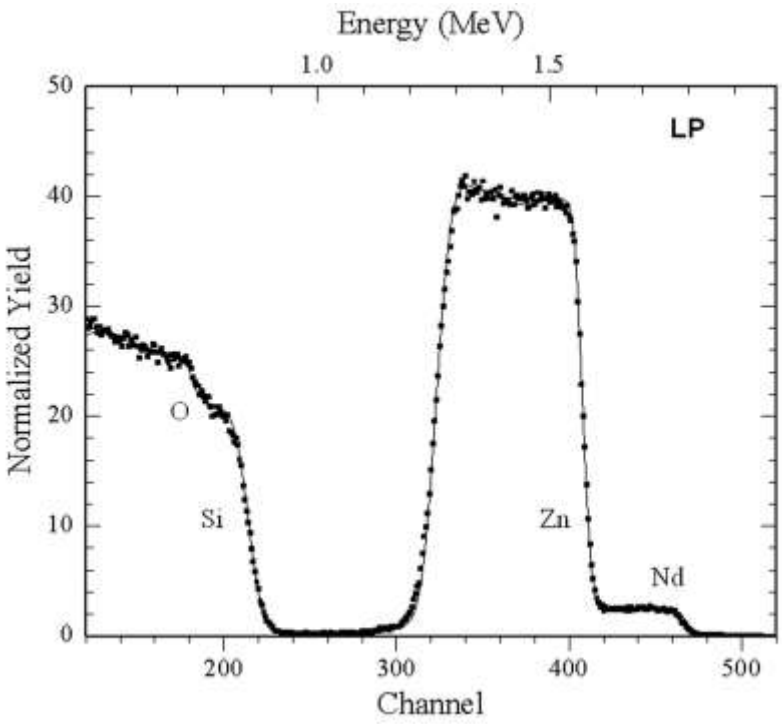
Energy (MeV)
1.0
1.5
LP
Normalized Yield
Channel
O
Si
Zn
Nd

b

Fig. 1

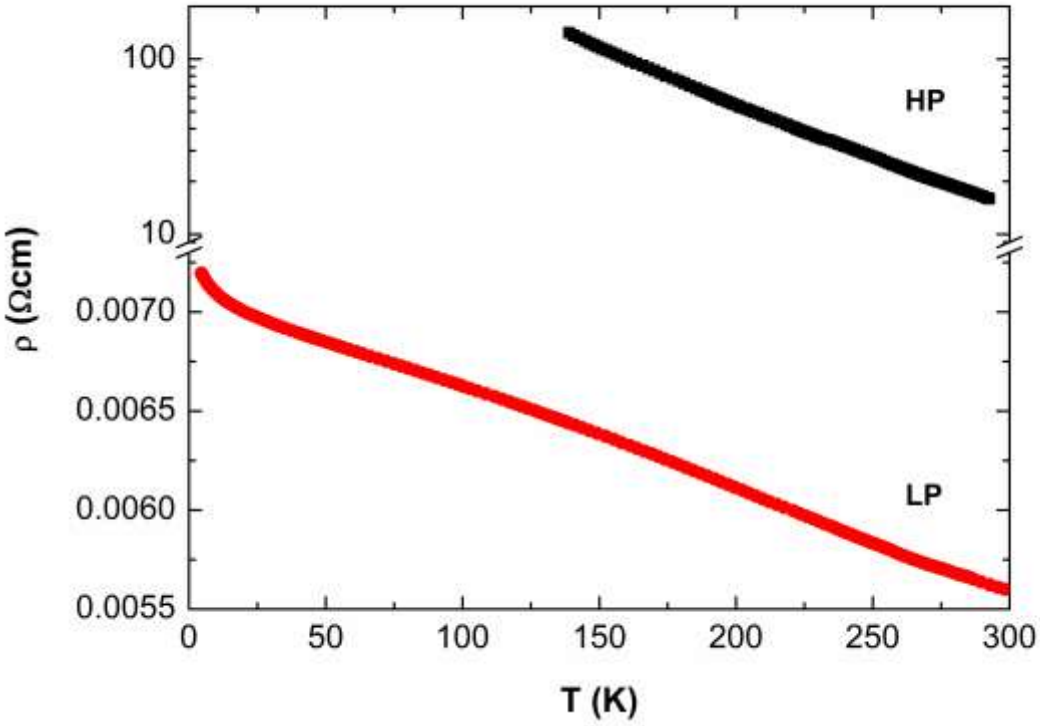
100
10
0.0070
0.0065
0.0060
0.0055
ρ (Ωcm)
HP
LP
0
50
100
150
200
250
300
T (K)

Fig. 2

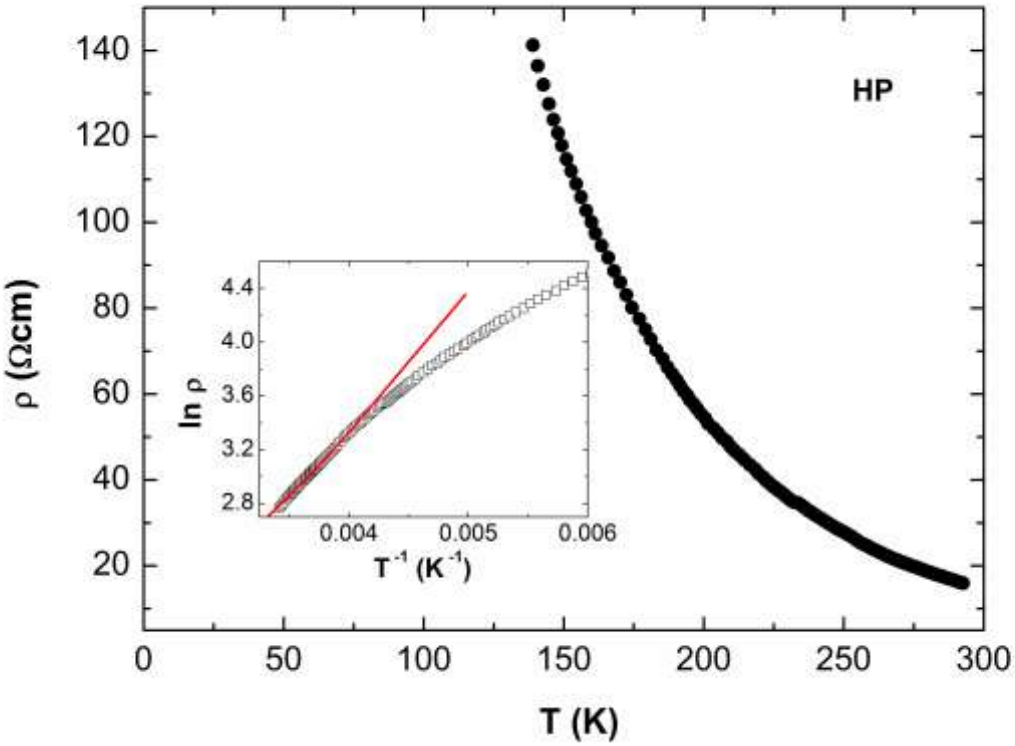
HP
ρ (Ωcm)
T (K)
ln ρ
T⁻¹ (K⁻¹)
140
120
100
80
60
40
20
0
50
100
150
200
250
300
4.4
4.0
3.6
3.2
2.8
0.004
0.005
0.006

Fig. 3

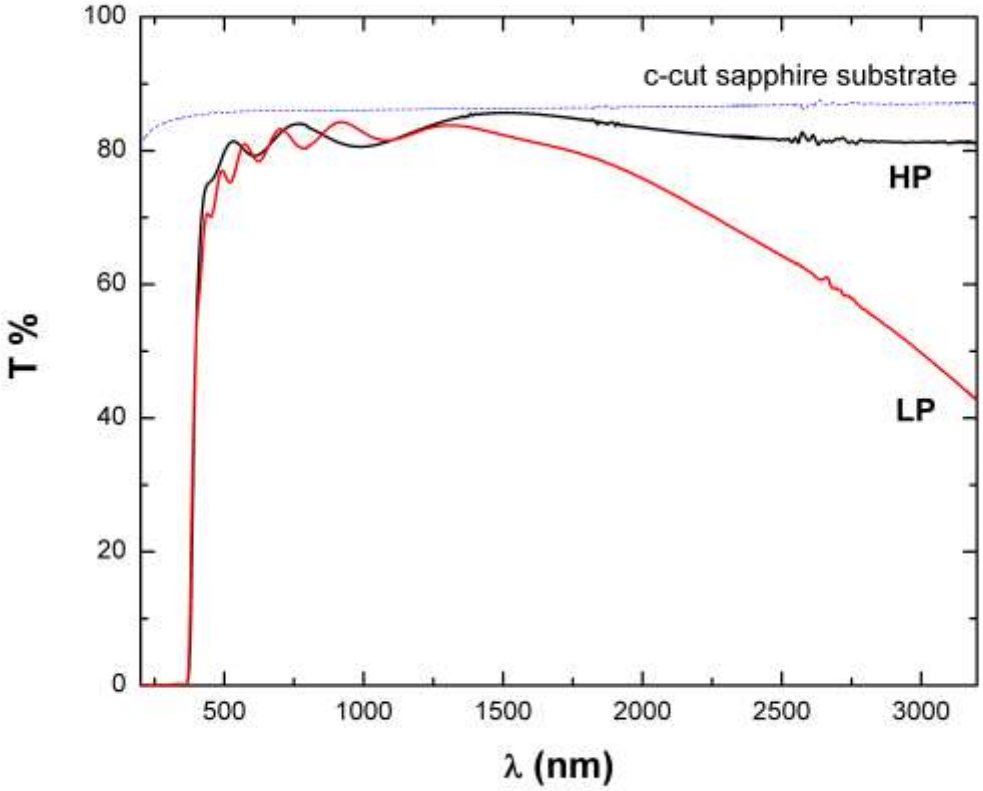
100
80
60
40
20
0
T %
500
1000
1500
2000
2500
3000
λ (nm)
c-cut sapphire substrate
HP
LP

Fig. 4a

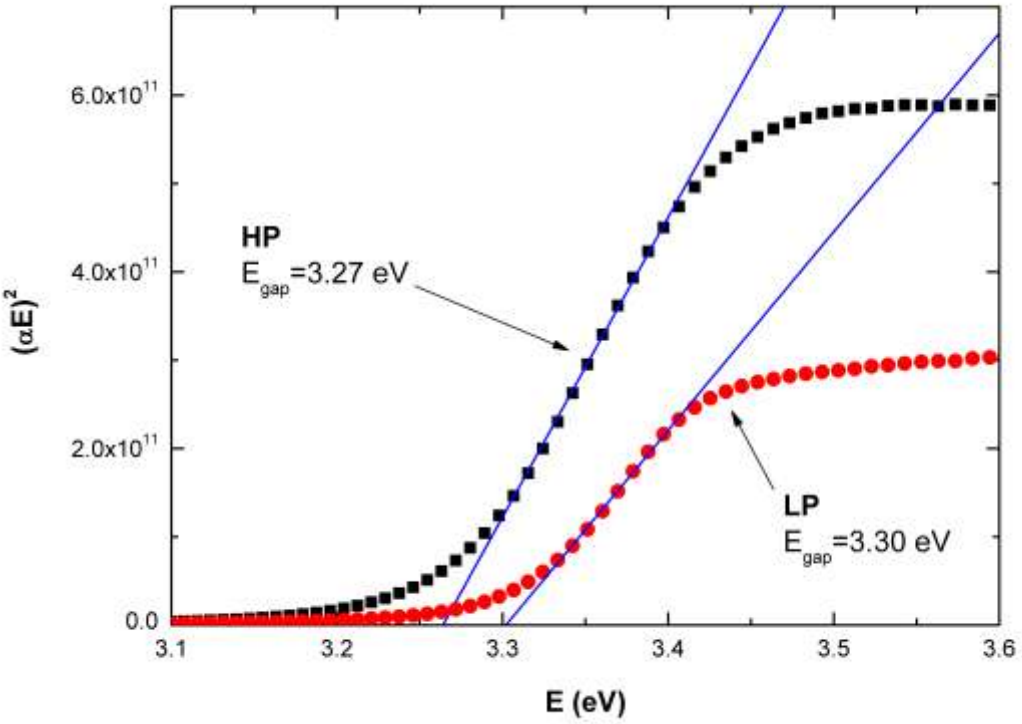
6.0x10^11
4.0x10^11
2.0x10^11
0.0
(αE)^2
HP
E_gap=3.27 eV
LP
E_gap=3.30 eV
3.1
3.2
3.3
3.4
3.5
3.6
E (eV)

Fig. 4b

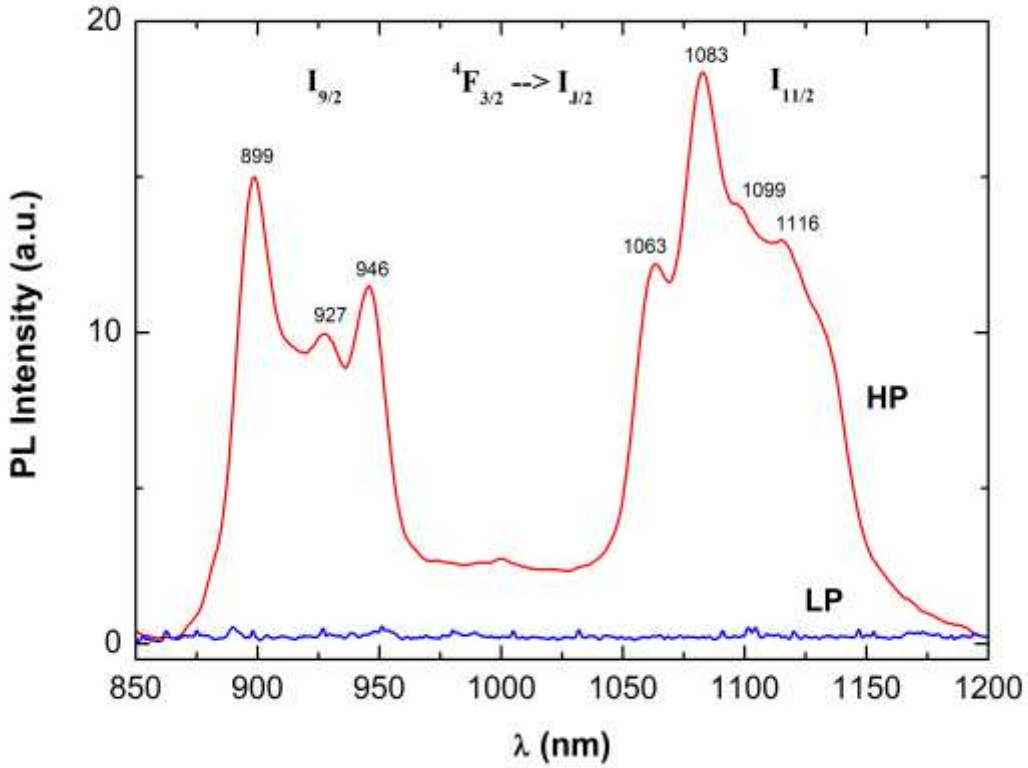
20
10
0
PL Intensity (a.u.)
850
900
950
1000
1050
1100
1150
1200
λ (nm)
I9/2
4F3/2 --> IJ/2
I11/2
899
927
946
1063
1083
1099
1116
HP
LP

Fig. 5a

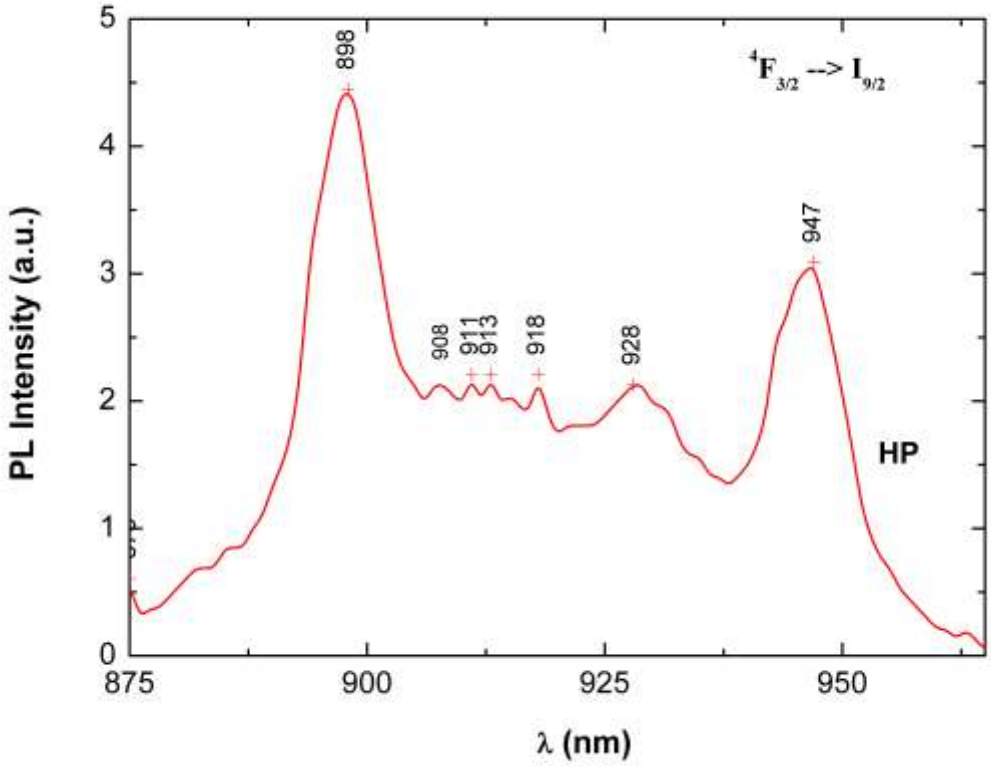
PL Intensity (a.u.)
λ (nm)
898
908
911
913
918
928
947
$^4F_{3/2}$ --> $I_{9/2}$
HP
0
1
2
3
4
5
875
900
925
950

Fig 5b

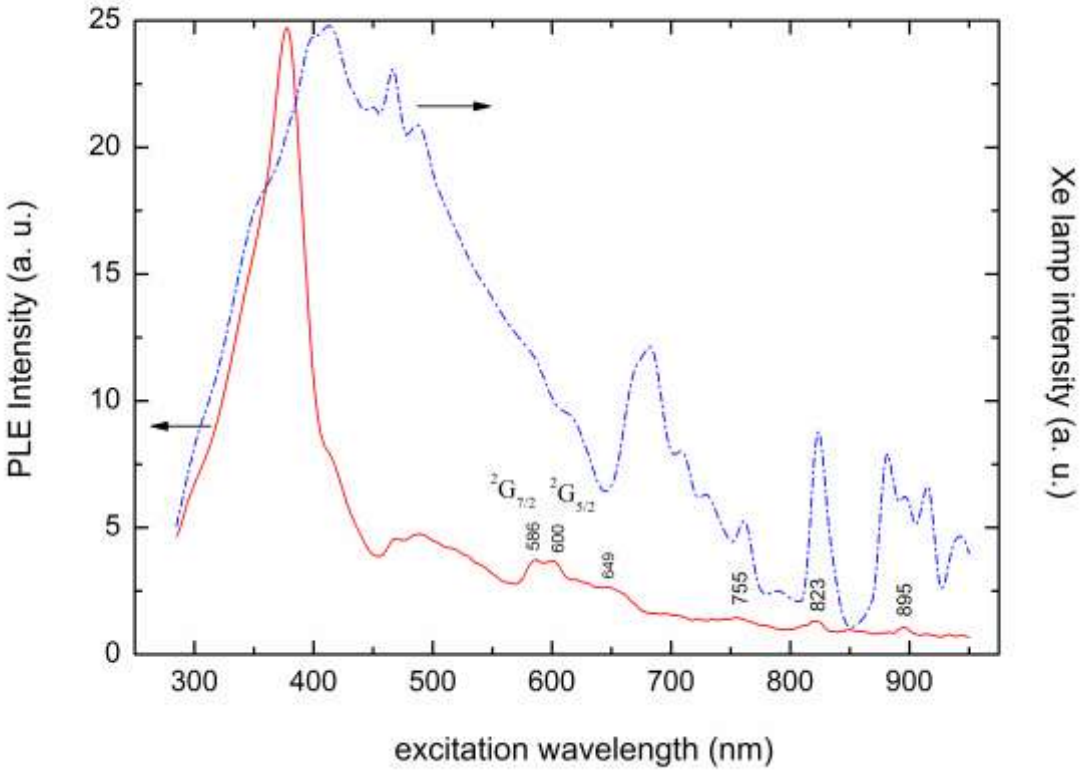
PLE Intensity (a. u.)
Xe lamp intensity (a. u.)
excitation wavelength (nm)
0
5
10
15
20
25
300
400
500
600
700
800
900
$^2G_{7/2}$
$^2G_{5/2}$
586
600
649
755
823
895

Fig 6